symmetry

MDPI

Article

High Circular Dichroism Optical Chiral Metasurfaces Based on Bound States in the Continuum

Ziang Gao, Pu Wang, Shilin Yu, Zhengshan Xu and Tonggang Zhao *

School of Electronic Engineering, Beijing University of Posts and Telecommunications, Beijing 100876, China; zagao@bupt.edu.cn (Z.G.); 2021110466@bupt.cn (P.W.); yushilin@bupt.edu.cn (S.Y.); hyxzs@bupt.edu.cn (Z.X.)
* Correspondence: zhaotg@bupt.edu.cn

Abstract: In this paper, we suggest a design for a chiral metasurface at optical frequencies that shows a high level of circular dichroism (CD) of 0.94. By breaking the in-plane asymmetry and exciting the quasi-bound states in the continuum (quasi-BICs), a high Q-factor was obtained, which greatly enhances the interaction between light and matter. Then, the multipole decomposition was confirmed to analyze its mode of excitation. The proposed design may provide new possibilities for high-performance optical devices.

Keywords: chiral metasurface; circular dichroism

Citation: Gao, Z.; Wang, P.; Yu, S.; Xu, Z.; Zhao, T. High Circular Dichroism Optical Chiral Metasurfaces Based on Bound States in the Continuum. *Symmetry* **2023**, *15*, 1444. https://doi.org/10.3390/sym15071444

Academic Editors: Ming Yan and Alexey V. Lukoyanov

Received: 20 June 2023
Revised: 16 July 2023
Accepted: 18 July 2023
Published: 19 July 2023

1. Introduction

Two-dimensional (2D) metamaterials, or synthetic materials with a thickness less than the working wavelength, are known as metasurfaces. The majority of conventional metamaterials use valuable metals as a medium to achieve surface plasmon resonance, which results in light waves with various characteristics at various frequencies in terms of reflection, transmission, and absorption [1]. The metasurface scale is minuscule in comparison to synthetic three-dimensional (3D) metamaterials. It can make possible the management of the amplitude, phase, polarization, and other features of incident light, which has drawn a great deal of attention, by assembling metaatoms with specific electromagnetic properties in diverse ways to produce a two-dimensional planar structure. Researchers have become fascinated with optical devices based on all-dielectric metasurfaces because of its low loss, affordable production costs, straightforward manufacturing methods and high compatibility with Complementary Metal Oxide Semiconductors (CMOS) [2].

Chirality is an inherent characteristic of chiral molecules and a manifestation of vital signs, which are ubiquitous in the organic world [3–5]. However, in nature, there are very few chiral structures for achieving specific functions, and the relevant modeling and theoretical analysis are limited to the characterization of the original structure. At present, the research on chiral metamaterials is gradually expanding from the microwave band to the terahertz, infrared, and even optical bands [4,6,7].

With the development of the field of optical metasurfaces, chiral metasurfaces have also received widespread attention and research, with studies mainly utilizing micro- and nanostructures to generate strong chiral optical responses at subwavelength thicknesses [8,9]. Chirality refers to the characteristic in geometry where the mirror image of an object cannot coincide with itself. Chiral materials can be divided into natural chiral materials and artificial chiral materials [10–12]. If an object is different from its mirror image, it is called 'chiral', and its mirror image cannot overlap with the original object, just as the left and right hands are mirror images of each other and cannot overlap. Detecting chiral signals in substances has become a hot research topic for researchers. However, the existing chiral metasurfaces, whether dielectronic or based on plasmons, still produce weak circular dichroism (CD) signals [13–15]. In 2022, Jie Gao's research group experimentally demonstrated the selective CD in dual bands of

4–5 μm and 5–6 μm. This structure provides dual-band regulation, but the CD did not reach a high level (close to 0.6) [16]. In 2023, Xiangkai Zeng et al. proposed a chiral metasurface that displays a high CD value of greater than 0.57 as the chiral plasmonic resonance wavelength varies from 4.96 μm to 5.82 μm [17]. This structure provides a high CD for a single band, but it fails to achieve dual-band regulation.

More importantly, the quality factor (Q-factor) of the resonance peak is not high, resulting in limited intrinsic chiral interaction between light and matter. Bound states in the continuum (BICs), electromagnetic eigenstates that exist in the radiative continuous spectrum but still remain localized, have the characteristics of maximum Q-factor and strong interactions between light and matter [18–20]. BICs comprise a special resonance mode in the metasurface whose frequency is located in the radiation continuous domain but is completely bound without any energy leakage. In theory, such a state has an infinite Q-factor, and it could be widely used to enhance the interaction between light and matter in various fields, such as ultra-low threshold lasers, enhanced nonlinear optical effects, and enhanced chiral optical responses. They are generally divided into two patterns: symmetry-protected BICs [21] and accidental BICs [22]. Ultra-sensitive sensing has received great attention in recent years. However, because the resonance linewidth of the ideal BIC is zero, although the energy can be perfectly bound, it is invisible in the spectrum. Therefore, only by transforming BICs into quasi-bound states in the continuum (quasi-BICs) can observation be guaranteed. At present, the main way to obtain quasi-BICs is to break the shape or size symmetry of nanoparticles [23]. In order to obtain an ultra-high Q-factor, the asymmetry factor must be very small [24], which puts forward extremely stringent requirements for nanoprocessing and greatly limiting the application of quasi-BICs in the real world [25]. In 2022, a new method for the formation of quasi-BICs was created which breaks the structural symmetry in the lattice units by adjusting the relative displacement of nanoparticles in the metasurface. This method reduces processing difficulty without changing the size and shape of the nanoparticles, laying the foundation for the practical application of quasi-BICs [26–28].

We believe that planar chiral metasurfaces controlled by BIC physics may have many applications in chiral lasers, nonlinear filters, and other active chiral optical devices. A chiral BIC is completely decoupled from circularly polarized light in one spin direction and strongly interacts with circularly polarized light in another spin direction, producing the largest CD and an extremely high Q-factor at the same time.

In this paper, we propose a design for a novel chiral metasurface based on etching silicon blocks with two quarter-elliptical cylinders. Transferring the BIC to quasi-BICs is the recommended approach for constructing the structure with intrinsic planar chirality. The physical mechanism of the process of transitioning from a symmetry-protected BIC to quasi-BICs is that when the symmetry of the metasurface is disrupted, new radiation channels are established, allowing this mode to have a relatively tiny resonant linewidth and a high Q-factor because it can radiate to the external continuum. The leakage of energy enables the BIC to complete the transition to quasi-BICs. We defined the degree of asymmetry δ. By calculating the area difference between the two etched apertures, it was found that the structure satisfies the inverse square law, which verifies the excitation of the quasi-BIC modes. After parameter adjustment, the maximum CD value of this structure was 0.94. Meanwhile, we utilized the electromagnetic multipole decomposition method to analyze the dominant electromagnetic modes as electric dipole and magnetic dipole modes. This study is of great significance in promoting the interaction between light and matter and enhancing chiral sensing.

2. Structure Design

In Figure 1a, the parameters and details of the metasurface structure are displayed. The structural unit cell is a cubic silicon block on which two quarter-elliptical cylinders are etched. The substrate is glass, and the material data is referenced in the Palik manual [29]. It is surrounded by a gas environment with a refractive index of 1. The period of the unit

cell is 850 nm. The plane wave electric field is incident perpendicular to the metasurface and polarized along the x-axis (polarization angle θ = 0°).

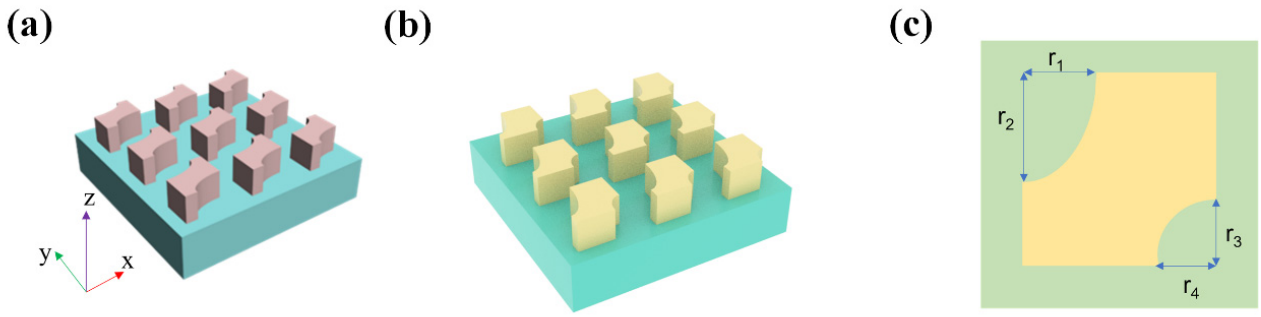

Figure 1. (**a**) Schematic diagram of the designed symmetric all-dielectric metasurface. (**b**) Schematic diagram of the designed asymmetric all-dielectric metasurface. (**c**) Top view of the unit cell of the asymmetric all-dielectric metasurface. Geometric parameters are shown in the figure.

By changing the major and minor axes of the ellipse (r_1, r_2, r_3, r_4), the symmetry within the plane is broken, as shown in Figure 1b. To better illustrate the asymmetric structure, the top view of the unit cell is drawn as shown in Figure 1c.

Equations (1) and (2) define in-plane geometry symmetry breaking parameter δ and asymmetry parameter α:

$$\delta = \frac{\pi r_1 r_2}{4} - \frac{\pi r_3 r_4}{4} \quad (1)$$

$$\alpha = \frac{\delta}{S} \quad (2)$$

where S is the area of the square silicon block.

We calculated the optical properties of this structure using the finite-difference time domain (FDTD) method, and due to its repeating design, obtaining the response only required simulation of a single period with a periodical boundary condition in the x and y directions and perfectly matched layers (PMLs) in the z direction [26,30].

3. Results and Discussion

The measured parameters of the simulated incident circularly polarized light with different rotations under symmetric conditions are shown in Figure 2a. T_{rl} represents the right-handed component transmitted when the left-handed circularly polarized light is incident, r represents RCP, and l represents LCP [31]. There is no resonance with $T_{rl} = T_{lr}$ and $T_{ll} = T_{rr}$ due to reciprocity, and CD = 0. This state is symmetry-protected BIC.

The symmetry-protected BIC largely depends on the geometric symmetry of the structure. The electromagnetic waves of the BIC remain completely localized in space, and theoretically their lifespan can become infinitely long, even if they reside in a continuous spectrum of extended states. This special optical confinement phenomenon stems from the special solution of the Wave Equation, in which the wave function is localized in the radiation band. BIC is a dark mode embedded in the parameter space, exhibiting an infinite-radiation Q-factor.

In Figure 2b, we generated asymmetry by adjusting the major and minor axes of two ellipses, and we excited two modes at 1431.1 nm (mode I) and 1574.7 nm (mode II), respectively. In mode I, the component T_{rr} was significantly higher than the other components T_{rl}, T_{ll} and T_{lr}. In mode II, the components T_{rl} and T_{ll} were significantly higher than the other components T_{rr} and T_{lr}. The CD values are shown in Figure 2c.

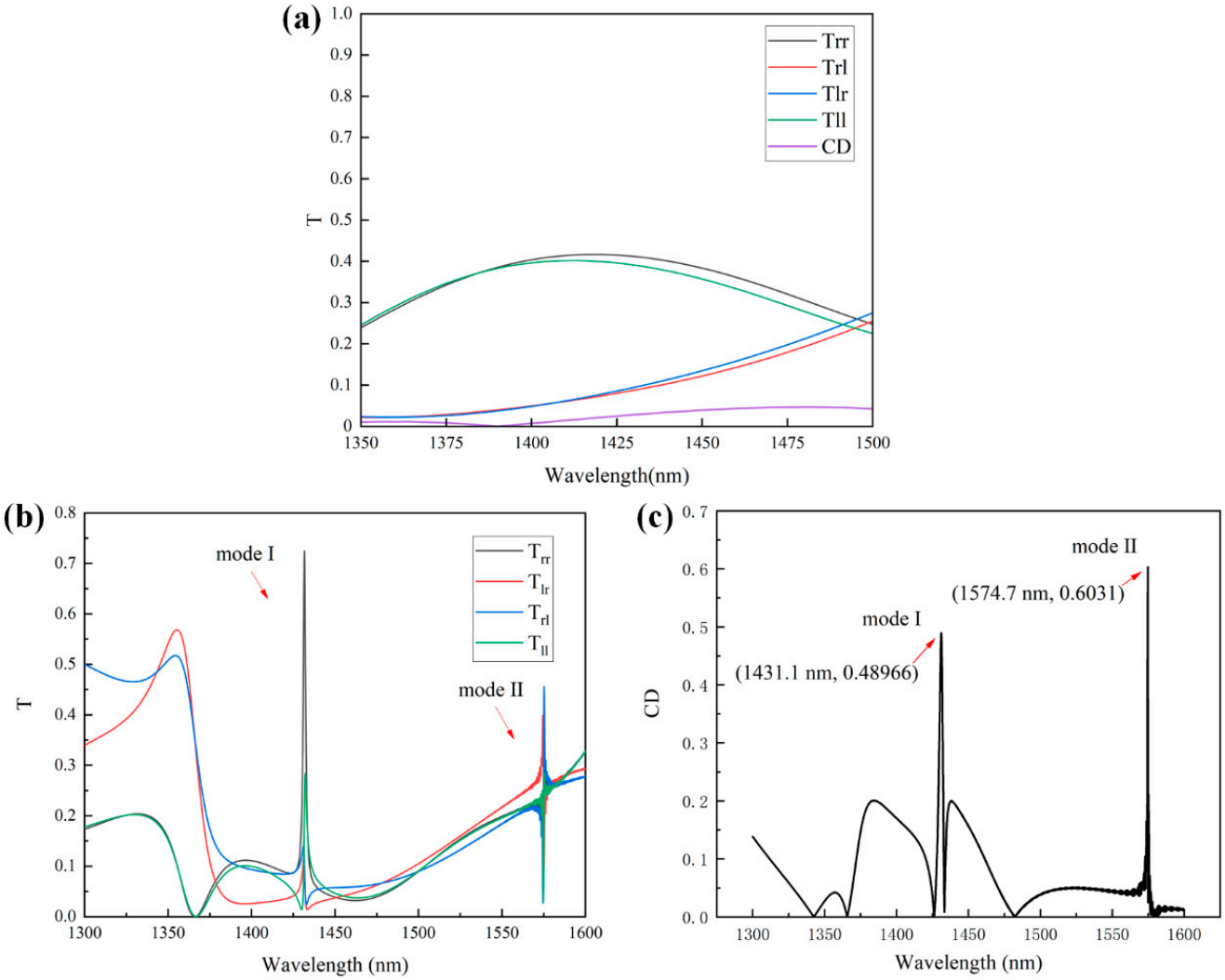

Figure 2. (**a**) Simulated transmission Jones matrix spectra and CD values for symmetric metasurfaces (r_1 = 440 nm, r_2 = 200 nm, r_3 = 440 nm, r_4 = 200 nm, $\delta = 0$) (**b**). Simulated transmission Jones matrix spectra for asymmetric metasurfaces (r_1 = 440 nm, r_2 = 200 nm, r_3 = 200 nm, r_4 = 240 nm, $\delta = \frac{\pi \times 440 \times 200}{4} - \frac{\pi \times 200 \times 240}{4} = \pi \times 10^4$). (**c**) Simulated transmission CD values for asymmetric metasurfaces.

Here, the CD is defined as the transmittance difference under right-handed polarization (RCP) and left-handed polarization (LCP) incidence [32].

$$CD = \frac{|(T_{rr} + T_{lr}) - (T_{rl} + T_{ll})|}{(T_{rr} + T_{lr}) + (T_{rl} + T_{ll})} \tag{3}$$

We performed simulated computations to examine the impact of structural factors on the CD values of chiral metasurfaces. As shown in Figure 3a, we found that in this design, as thickness increased, the CD values of both modes showed a decreasing trend, and the position of mode resonance also underwent a red shift.

Furthermore, we changed the radius of the lower ellipse to achieve another structural design under asymmetric parameters. The specific parameters are as follows: r_3 = 280 nm; r_4 = 320 nm.

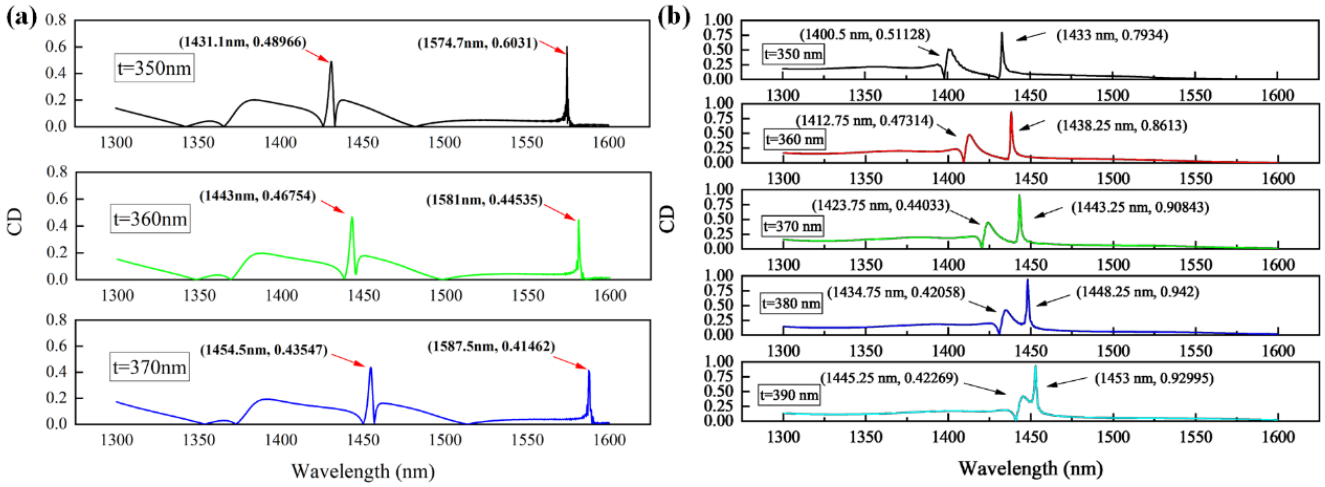

Figure 3. (**a**) Simulated transmission CD values for asymmetric metasurfaces with different thicknesses (r_1 = 440 nm, r_2 = 200 nm, r_3 = 200 nm, r_4 = 240 nm, $\delta = \frac{\pi \times 440 \times 200}{4} - \frac{\pi \times 200 \times 240}{4} = \pi \times 10^4$). (**b**) Simulated transmission CD values for asymmetric metasurfaces with different thicknesses (r_1 = 440 nm, r_2 = 200 nm, r_3 = 280 nm, r_4 = 320 nm, $|\delta| = \left|\frac{\pi \times 440 \times 200}{4} - \frac{\pi \times 280 \times 320}{4}\right| = 400\pi$).

Similar to this, we changed the thickness t and discovered that the CD value of mode II increased as thickness did as well. Both modes exhibited a red shift at the same moment, although mode I had a wider range of motion, bringing the two modes closer together. As shown in Figure 3b, we found that the CD value of mode II continuously increased with increasing thickness, with 380 nm being the critical maximum value (CD = 0.942).

We carried out an investigation of the period parameters to look into how the CD of the structure changed, as shown in Figure 4. When the period gradually increased from 840 nm to 860 nm, both of the modes underwent a red shift. However, regarding CD values, that of mode I climbed gradually, whereas that of mode II increased initially and subsequently decreased.

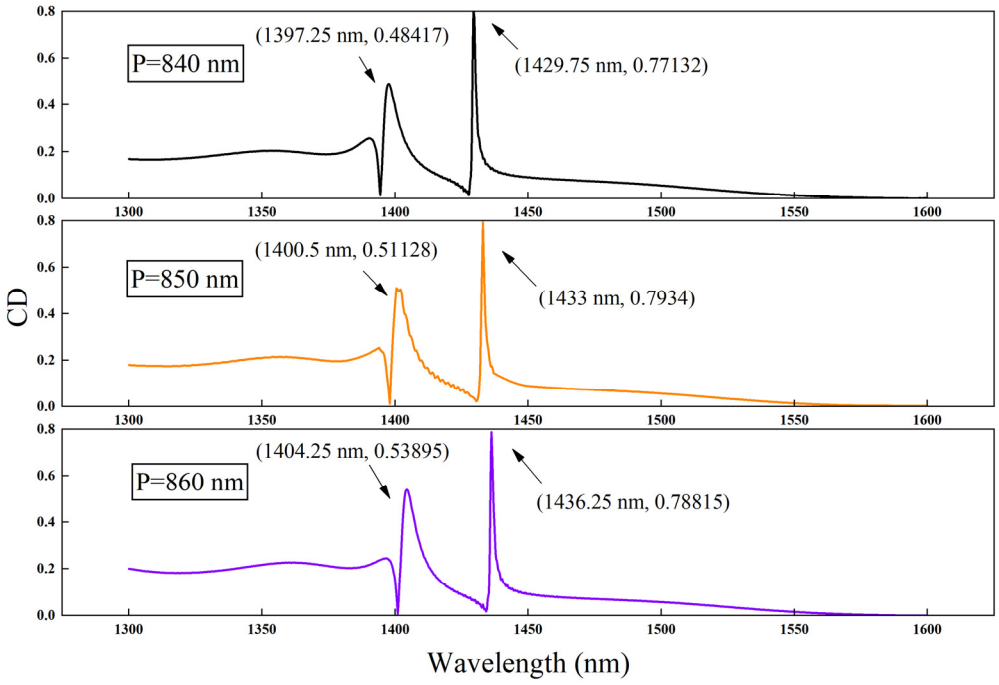

Figure 4. Simulated transmission CD values for asymmetric metasurfaces with different periods (r_1 = 440 nm, r_2 = 200 nm, r_3 = 280 nm, r_4 = 320 nm, $|\delta| = \left|\frac{\pi \times 440 \times 200}{4} - \frac{\pi \times 280 \times 320}{4}\right| = 400\pi$).

An essential tool for examining how electromagnetic fields interact with material systems is multipole decomposition. In all forms of all-dielectric metasurface spectroscopy, it can aid in understanding the physical mechanisms of resonant mode formation. The source's multipole moment effectively captures all the details of electromagnetic field coupling and radiation for a specific charge density distribution. The multipole moment of the charge current distribution completely describes the electromagnetic radiation of the source and the coupling of the external field to it. Each multipole moment is uniquely coupled to a corresponding multipole field.

In the Cartesian coordinate system, the form of multipole moments is [33]:

Electric dipole (ED) moment

$$\vec{P} = \frac{1}{i\omega} \int \vec{j} \, d^3r \tag{4}$$

Magnetic dipole (MD) moment

$$\vec{M} = \frac{1}{2c} \int (\vec{r} \times \vec{j}) d^3r \tag{5}$$

Toroidal dipole (TD) moment

$$\vec{T} = \frac{1}{10c} \int \left[(\vec{r} \cdot \vec{j}) \vec{r} - 2r^2 \vec{j} \right] d^3r \tag{6}$$

Electric quadrupole (EQ) moment

$$Q_{\alpha\beta} = \frac{1}{i\omega} \int \left[r_\alpha j_\beta + r_\beta j_\alpha - \frac{2}{3} (\vec{r} \cdot \vec{j}) \right] d^3r \tag{7}$$

Magnetic quadrupole (MQ) moment

$$M_{\alpha\beta} = \frac{1}{3c} \int \left[(\vec{r} \times \vec{j})_\alpha r_\beta + (\vec{r} \times \vec{j})_\beta r_\alpha \right] d^3r \tag{8}$$

where $\vec{j}$ is the displacement current vector, $\vec{r}$ is the position vector, ω is angular frequency, and c is the speed of light in vacuum.

E. Radescu and G. Vaman derive the total radiant intensity of the far field as follows:

$$\begin{aligned} I_{sca} = \frac{2\omega^4}{3c^3} |\vec{P}|^2 + \frac{2\omega^4}{3c^3} |\vec{M}|^2 + \frac{2\omega^6}{3c^5} |\vec{T}|^2 + \frac{4\omega^5}{3c^4} (\vec{P} \cdot \vec{T}) + \frac{\omega^6}{5c^5} Q_{\alpha\beta} Q_{\alpha\beta} + \\ \frac{\omega^6}{20c^5} M_{\alpha\beta} M_{\alpha\beta} + \frac{2\omega^6}{15c^5} (\vec{M} \cdot \langle \vec{R}^2_{\vec{M}} \rangle) + o\left(\frac{1}{c^5}\right) \end{aligned} \tag{9}$$

Among them, the first and second terms correspond to the scattering of ED and MD multipoles, the third term corresponds to the scattering of TD multipoles, and the fourth term is the interference between ED multipoles and TD multipoles.

Following calculation, Figure 5 displays the fundamental electromagnetic source dispersion. It is evident from the graphic that mode I was dominated by ED, whereas mode II was dominated by MD.

In the case of asymmetry, the structure can produce a new Fano peak, and its transmission spectrum can thereby be fitted using the Fano formula [34]:

$$T_{Fano} = \left| a_1 + ia_2 + \frac{b}{\omega - \omega_0 + i\gamma} \right|^2 \tag{10}$$

where a_1, a_2, and b are constants, ω_0 is the resonant frequency, and γ is the damping ratio of the resonant cavity.

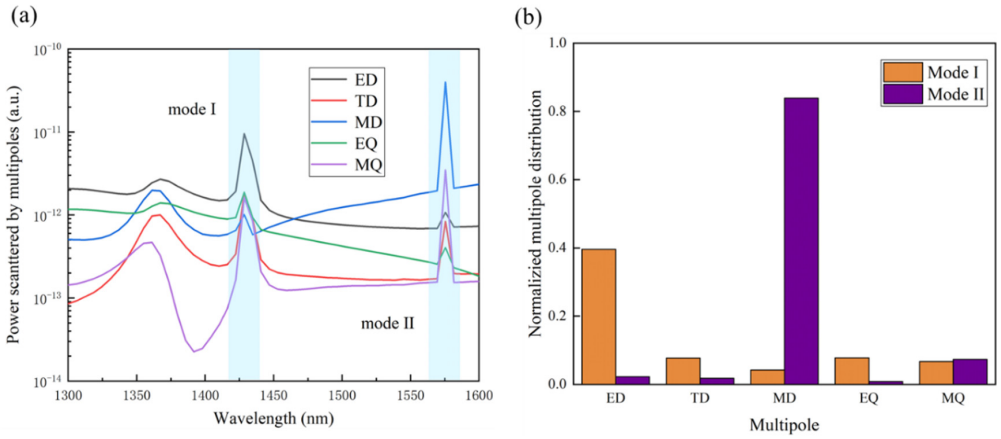

Figure 5. (**a**) Radiation intensities from different multipoles for mode I and mode II on a logarithmic scale. (**b**) Normalized multiple distributions from different multipoles for mode I and mode II.

The Q-factor is calculated as follows [35]:

$$Q = \frac{\omega_0}{2\gamma} \tag{11}$$

The deep relationship between the radiative Q-factors and the asymmetric parameters is revealed by the following formula:

$$Q \propto \alpha^{-2} \tag{12}$$

By using this method, we can obtain different asymmetric parameters. Here, asymmetric parameters can be defined as $\alpha = \Delta S/S$, where S is the area of the unit molecule and ΔS is the area of the asymmetric part. Therefore, the Q-factor of the resonance mode can be expressed as:

$$Q = \frac{A}{2k_0}|p_0|^{-2}(\alpha)^{-2} \tag{13}$$

where p_0 is the electric dipole moment at the bottom of the elementary molecule, A is the area of the periodic unit, and k_0 is the wave vector along the z-axis [25,36].

As shown in Figure 6, curve fitting was performed in a logarithmic coordinate system, and the slope of the curve was close to -2. Therefore, it can be verified that this mode was a quasi-BIC.

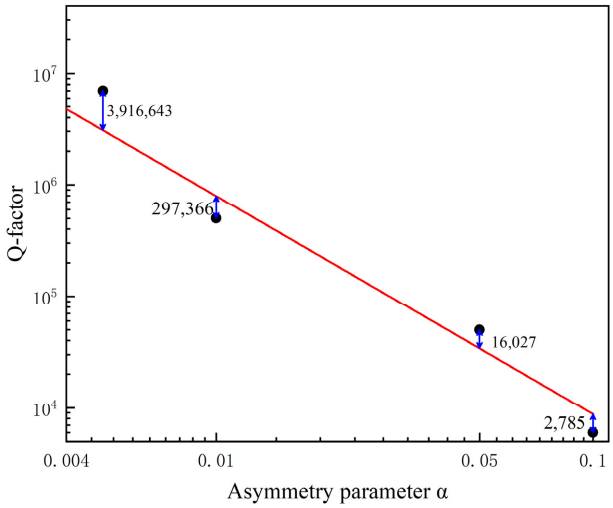

Figure 6. Q-factors of the planar chiral q-BIC mode on the relative asymmetry parameter. (Blue arrows indicate difference between data points and fitted curves).

4. Conclusions

In this paper, we propose a novel chiral metasurface. The unit cell was etched two nanoholes from Si metasurface. Breaking the symmetry of the structure provided a radiation channel for the metasurface device, thereby stimulating the quasi-BIC resonance mode with a high *Q*-factor. An optical cavity with a high *Q*-factor can greatly enhance the interaction between light and matter. By introducing in-plane structural asymmetry, intrinsic planar chirality can be achieved under normal incidence with a maximum CD value of 0.94 at optical frequency. The proposed optical metasurface has the advantages of a simple structure, easy integration, and good robustness, and it is expected to have potential value in high-performance chiral sensing.

Author Contributions: Conceptualization, Z.G.; Methodology, Z.G.; Software, Z.G.; Validation, Z.G.; Investigation, S.Y.; Data curation, Z.G.; Writing—original draft, Z.G.; Writing—review & editing, Z.X.; Visualization, P.W.; Funding acquisition, T.Z. All authors have read and agreed to the published version of the manuscript.

Funding: This research was funded by [National Key Research and Development Program of China] grant number [2022YFF0707104] and [BUPT Excellent Ph.D. Students Foundation] grant number [CX2023XXX]. And The APC was funded by [National Key Research and Development Program of China] grant number [2022YFF0707104].

Institutional Review Board Statement: Not applicable.

Informed Consent Statement: Not applicable.

Data Availability Statement: Not applicable.

Conflicts of Interest: The authors declare no conflict of interest.

References

1. Meinzer, N.; Barnes, W.L.; Hooper, I.R. Plasmonic meta-atoms and metasurfaces. *Nat. Photonics* **2014**, *8*, 889–898. [CrossRef]
2. Tseng, M.L.; Jahani, Y.; Leitis, A.; Altug, H. Dielectric metasurfaces enabling advanced optical biosensors. *ACS Photonics* **2020**, *8*, 47–60. [CrossRef]
3. Zhao, Y.; Askarpour, A.N.; Sun, L.; Shi, J.; Li, X.; Alù, A. Chirality detection of enantiomers using twisted optical metamaterials. *Nat. Commun.* **2017**, *8*, 14180. [CrossRef] [PubMed]
4. Chela-Flores, J. Comments on a novel approach to the role of chirality in the origin of life. *Chirality* **1991**, *3*, 389–392. [CrossRef]
5. Ben Moshe, A.; Szwarcman, D.; Markovich, G. Size dependence of chiroptical activity in colloidal quantum dots. *ACS Nano* **2011**, *5*, 9034–9043. [CrossRef] [PubMed]
6. Berova, N.; Polavarapu, P.L.; Nakanishi, K.; Woody, R.W. *Comprehensive Chiroptical Spectroscopy: Applications in Stereochemical Analysis of Synthetic Compounds, Natural Products, and Biomolecules*; John Wiley & Sons: Hoboken, NJ, USA, 2012.
7. Tsukube, H.; Shinoda, S. ChemInform Abstract: Lanthanoid Complexes in Molecular Recognition and Chirality Sensing of Biological Substrates. *ChemInform* **2002**, *33*, 2389–2404. [CrossRef]
8. McKendry, R.; Theoclitou, M.-E.; Rayment, T.; Abell, C. Chiral discrimination by chemical force microscopy. *Nature* **1998**, *391*, 566–568. [CrossRef]
9. Haesler, J.; Schindelholz, I.; Riguet, E.; Bochet, C.G.; Hug, W. Absolute configuration of chirally deuterated neopentane. *Nature* **2007**, *446*, 526–529. [CrossRef]
10. Schreiber, R.; Luong, N.; Fan, Z.; Kuzyk, A.; Nickels, P.C.; Zhang, T.; Smith, D.M.; Yurke, B.; Kuang, W.; Govorov, A.O.; et al. Chiral plasmonic DNA nanostructures with switchable circular dichroism. *Nat. Commun.* **2013**, *4*, 2948. [CrossRef]
11. Hentschel, M.; Schäferling, M.; Duan, X.; Giessen, H.; Liu, N. Chiral plasmonics. *Sci. Adv.* **2017**, *3*, e1602735. [CrossRef]
12. Schnell, M.; Sarriugarte, P.; Neuman, T.; Khanikaev, A.B.; Shvets, G.; Aizpurua, J.; Hillenbrand, R. Real-space mapping of the chiral near-field distributions in spiral antennas and planar metasurfaces. *Nano Lett.* **2016**, *16*, 663–670. [CrossRef] [PubMed]
13. Fedotov, V.A.; Mladyonov, P.L.; Prosvirnin, S.L.; Rogacheva, A.V.; Chen, Y.; Zheludev, N.I. Asymmetric Propagation of Electromagnetic Waves through a Planar Chiral Structure. *Phys. Rev. Lett.* **2006**, *97*, 167401. [CrossRef]
14. Konishi, K.; Sugimoto, T.; Bai, B.; Svirko, Y.; Kuwata-Gonokami, M. Effect of surface plasmon resonance on the optical activity of chiral metal nanogratings. *Opt. Express* **2007**, *15*, 9575–9583. [CrossRef] [PubMed]
15. Cao, T.; Qiu, Y. Lateral sorting of chiral nanoparticles using Fano-enhanced chiral force in visible region. *Nanoscale* **2018**, *10*, 566–574. [CrossRef] [PubMed]
16. Tang, H.; Rosenmann, D.; Czaplewski, D.A.; Yang, X.; Gao, J. Dual-band selective circular dichroism in mid-infrared chiral metasurfaces. *Opt. Express* **2022**, *30*, 20063–20075. [CrossRef] [PubMed]

17. Zeng, X.; Rosenmann, D.; Czaplewski, D.A.; Gao, J.; Yang, X. Chiral metasurfaces of wavy rectangle resonators with tunable circular dichroism. *Optik* **2023**, *286*, 171024. [CrossRef]
18. Alizadeh, M.; Reinhard, B.R.M. Plasmonically enhanced chiral optical fields and forces in achiral split ring resonators. *ACS Photonics* **2015**, *2*, 361–368. [CrossRef]
19. Tang, Y.; Cohen, A.E. Optical chirality and its interaction with matter. *Phys. Rev. Lett.* **2010**, *104*, 163901. [CrossRef]
20. Yin, X.; Schaferling, M.; Metzger, B.; Giessen, H. Interpreting chiral nanophotonic spectra: The plasmonic Born-Kuhn model. *Nano Lett.* **2013**, *13*, 6238–6243. [CrossRef]
21. Ni, L.; Wang, Z.; Peng, C.; Li, Z. Tunable optical bound states in the continuum beyond in-plane symmetry protection. *Phys. Rev. B* **2016**, *94*, 245148. [CrossRef]
22. Hsu, C.W.; Zhen, B.; Stone, A.D.; Joannopoulos, J.D.; Soljačić, M. Bound states in the continuum. *Nat. Rev.Mater.* **2016**, *1*, 16048. [CrossRef]
23. Fan, K.; Shadrivov, I.V.; Padilla, W.J. Dynamic bound states in the continuum. *Optica* **2019**, *6*, 169–173. [CrossRef]
24. Friedrich, H.; Wintgen, D. Interfering resonances and bound states in the continuum. *Phys. Rev. A* **1985**, *32*, 3231–3242. [CrossRef] [PubMed]
25. Koshelev, K.; Lepeshov, S.; Liu, M.; Bogdanov, A.; Kivshar, Y. Asymmetric Metasurfaces with High-Q Resonances Governed by Bound States in the Continuum. *Phys. Rev. Lett.* **2018**, *121*, 193903. [CrossRef]
26. Algorri, J.F.; Dell'Olio, F.; Roldán-Varona, P.; Rodríguez-Cobo, L.; López-Higuera, J.M.; Sánchez-Pena, J.M.; Zografopoulos, D.C. Strongly resonant silicon slot metasurfaces with symmetry-protected bound states in the continuum. *Opt. Express* **2021**, *29*, 10374–10385. [CrossRef]
27. Li, B.; Yao, J.; Zhu, H.; Cai, G.; Liu, Q. Asymmetric excitations of toroidal dipole resonance and the magnetic dipole quasi-bound state in the continuum in an all-dielectric metasurface. *Opt. Mater. Express* **2021**, *11*, 2359–2368. [CrossRef]
28. He, Y.; Guo, G.; Feng, T.; Xu, Y.; Miroshnichenko, A.E. Toroidal dipole bound states in the continuum. *Phys. Rev. B* **2018**, *98*, 161112. [CrossRef]
29. Overvig, A.C.; Malek, S.C.; Carter, M.J.; Shrestha, S.; Yu, N. Selection rules for quasi-bound states in the continuum. *Phys. Rev. B* **2020**, *102*, 035434. [CrossRef]
30. Sadrieva, Z.F.; Sinev, I.S.; Koshelev, K.L.; Samusev, A.; Iorsh, I.V.; Takayama, O.; Malureanu, R.; Bogdanov, A.A.; Lavrinenko, A.V. Transition from optical bound states in the continuum to leaky resonances: Role of substrate and roughness. *ACS Photonics* **2017**, *4*, 723–727. [CrossRef]
31. Radescu, E.E.; Vaman, G.J.P.R.E. Exact calculation of the angular momentum loss, recoil force, and radiation intensity for an arbitrary source in terms of electric, magnetic, and toroid multipoles. *Phys. Rev. E* **2002**, *65*, 046609. [CrossRef]
32. Shi, T.; Deng, Z.L.; Geng, G.; Zeng, X.; Zeng, Y.; Hu, G.; Overvig, A.; Li, J.; Qiu, C.W.; Alù, A.; et al. Planar chiral metasurfaces with maximal and tunable chiroptical response driven by bound states in the continuum. *Nat. Commun.* **2022**, *13*, 4111. [CrossRef] [PubMed]
33. Papasimakis, N.; Fedotov, V.A.; Savinov, V.; Raybould, T.A.; Zheludev, N.I. Electromagnetic toroidal excitations in matter and free space. *Nat. Mater.* **2016**, *15*, 263–271. [CrossRef] [PubMed]
34. Yang, Y.; Kravchenko, I.I.; Briggs, D.P.; Valentine, J. All-dielectric metasurface analogue of electromagnetically induced transparency. *Nat. Commun.* **2014**, *5*, 5753. [CrossRef] [PubMed]
35. Xu, L.; Kamali, K.Z.; Huang, L.; Rahmani, M.; Smirnov, A.; Camacho-Morales, R.; Ma, Y.; Zhang, G.; Woolley, M.; Neshev, D.; et al. Dynamic Nonlinear Image Tuning through Magnetic Dipole Quasi-BIC Ultrathin Resonators. *Adv. Sci.* **2019**, *6*, 1802119. [CrossRef] [PubMed]
36. Li, S.; Zhou, C.; Liu, T.; Xiao, S. Symmetry-protected bound states in the continuum supported by all-dielectric metasurfaces. *Phys. Rev. A* **2019**, *100*, 063803. [CrossRef]